Supporting information

Unraveling Binding Effects of Cobalt(II) Sepulchrate with the Monooxygenase P450 BM-3 Heme Domain Using Molecular Dynamics Simulations

Rajni Verma[c], Ulrich Schwaneberg[d], Dirk Holtmann[e], Danilo Roccatano[a,b,*]

[a]School of Mathematics and Physics, University of Lincoln, Brayford Pool, Lincoln LN6 7TS, United Kingdom; [b]School of Engineering and Science, Jacobs University Bremen, Campus Ring 1, 28759 Bremen, Germany; [c]Department of Biomedical Engineering and Center for Biological Systems Engineering, Washington University in St. Louis, 63130 St. Louis, Missouri; [d]Department of Biotechnology, RWTH Aachen University, Worringer Weg 1, 52074 Aachen, Germany; [e]DECHEMA-Forschungsinstitut, Biochemical Engineering Group, Theodor-Heuss-Allee 25, 60486 Frankfurt am Main, Germany.

INDEX OF CONTENTS

TABLES

1) Table S1: GROMOS96 43a1 force field parameters for cobalt(II) sepulchrate.
2) Table S2: Partial charges on cobalt(II/III) sepulchrate for GROMOS96 43a1 force field.
3) Table S3: Number of different amino acids type with average SASA > 0.35 nm^2.
4) Table S4: Number of different amino acids type having a number of unique contacts with Co(II)Sep molecules.
5) Table S5: List of HEME residues involved in Co(II)Sep binding and involved in pathways with $k_{ET} > 0.1\ s^{-1}$.
6) Table S6: a) ET pathways with $k_{ET} > 10\ s^{-1}$ obtained from the 5CoS simulation. b) ET pathways with $k_{ET} > 10\ s^{-1}$ obtained from the 10CoS simulation. c) ET pathways with $k_{ET} > 10\ s^{-1}$ obtained from the 40CoS simulation.
7) Table S7: a) Co(II)Sep unbound/bound interaction energies for 5CoS and 10CoS simulations. b) Co(II)Sep unbound/bound interaction energies for 40CoS simulation.

FIGURES

1) Figure S1: Backbone root mean square deviation (RMSD) and radius of gyration (Rg) with respect to the crystal structure.
2) Figure S2: Minimum distance between P45C_α and A191C_α as a function of time.
3) Figure S3a,b: Contact occurrences of the Co(II)Sep molecules with the residues of heme domain.
4) Figure S4: Backbone RMSD matrix and cluster analysis.
5) Figure S5: Combined representation of ET pathways with $k_{ET} \geq 10\ s^{-1}$ obtained from 5CoS, 10CoS and 40CoS simulation.

TABLES

Table S1: Force field parameters for cobalt(II) sepulchrate adopted from the force constants calculated on the energy minimized geometries by Dehayes *et al*.[1]

Bond stretching parameters	
Bond type	**Force constant (kJ mol^{-1} nm^{-1})**
Co – N	885.234
N – C	2342.558
N – H	2962.824
C – C	2709.900
C – H	2740.010
Angle bending parameters	
Angle type	**Force constant (kJ mol^{-1} rad^{-2})**
N – Co – N	240.88
Co – N – C	167.41
Co – N – H	167.41
C – C – C	417.92
C – C – H	292.06
C – N – H	167.41
C – N – C	417.92
N – C – C	417.92
N – C – H	292.06
N – C – N	334.22
H – N – H	251.11
Dihedral parameters	
Dihedral type	**Force constant (kJ mol^{-1})**
H – C – C – H	2.729
H – C – N – Co	2.729
H – C – N – C	2.729
H – N – C – C	2.729

H – C – N – H	1.807
H – C – C – C	4.103
H – C – C – N	4.103
Co – N – C – C	1.373
N – Co – N – C	0.000
N – C – C – N	2.060
N – C – C – C	2.060
C – C – C – C	2.060

Table S2: Partial charges on cobalt(II/III) sepulchrate calculated by DFT calculations and adopted for GROMOS96 43a1 force field.[2]

Atom number	Atom type	Atom name	Charge group	Partial charge	
				Co(III)Sep	Co(II)Sep
1	CH2	C	1	0.283	0.514
2	N	N	2	-0.154	-0.544
3	CH2	C	3	0.147	0.149
4	CH2	C	4	0.147	0.149
5	N	N	5	-0.154	-0.542
6	CH2	C	6	0.283	0.511
7	N	N	7	-0.379	-0.945
8	CH2	C	8	0.284	0.639
9	N	N	9	-0.165	-0.785
10	CH2	C	10	0.120	0.143
11	CH2	C	11	0.202	0.253
12	N	N	12	-0.287	-0.944
13	CH2	C	13	0.320	0.697
14	N	N	14	-0.379	-0.947
15	CH2	C	15	0.284	0.639
16	N	N	16	-0.165	-0.785
17	CH2	C	17	0.120	0.143
18	CH2	C	18	0.202	0.253
19	N	N	19	-0.288	-0.944
20	CH2	C	20	0.321	0.697
21	CO	CO	21	1.043	1.682
22	H	H	22	0.184	0.252
23	H	H	23	0.225	0.381
24	H	H	24	0.199	0.351
25	H	H	25	0.225	0.381
26	H	H	26	0.198	0.351
27	H	H	27	0.184	0.251
Total Charges				3.0	2.0

Table S3. Number of different amino acids type with average SASA > 0.35 nm^2 calculated in the last 50 ns of the three simulations.

	WAT	**5CoS (I)**	**5CoS(II)**	**5CoS(III)**	**10CoS**	**40CoS**
Hydrophobic	37	38	45	36	35	40
Polar	45	47	40	41	46	47
Positive charged	45	47	49	46	50	48
Negative charged	54	58	54	59	55	58
Aromatic	14	12	16	17	15	12
Glycine	6	5	7	7	6	9
TOTAL	207	216	216	213	213	218

Table S4. Number of different amino acids type having a number of unique contacts larger than 6 with Co(II)Sep molecules. The averages have been calculated in the last 50 ns of each simulation.

Amino acid type	5CoS (I)	5CoS(II)	5CoS(III)	10CoS	40CoS
Hydrophobic	4	3	11	3	22
Polar	7	10	8	9	45
Positive charged	3	9	8	5	33
Negative charged	14	13	17	21	53
Glycine	0	0	0	0	0
Aromatic	1	0	4	5	15
TOTAL	29	35	48	43	168

Table S5. List of HEME residues involved in Co(II)Sep binding and pathways of ET rates values ≥ 0.1 s^{-1}. Asterisk in column 1 indicates the residues involved in pathways of ET rates values ≥10 s^{-1}. Third column reports secondary structure element in which amino acids is located. The fourth column report the maximum value of k_{ET} observed for the Co(II)Sep bound to this residue. Amino acids located in correspondence of HEME/FMN interface are indicated with 'X' in column 5. Columns 6-10 indicate Co(II)Sep binding to HEME residue. Last column indicates amino acid mutation(s) reported in literature for HEME residues involved in Co(II)Sep binding.

N.	Res. No.	Res. Name	Secondary Structure	Max $k_{ET}(s^{-1})$	Heme /FMN Inter.	5CoS (I)	5CoS (II)	5CoS (III)	10CoS	40CoS	Reported mutations
1	23*	ASP	coil-loop: lc1	174.8						30, 35, 38	
2	34	ASP	α -helix: A	7.7			3				
3	38	GLU	b-sheet: 1.1	0.3					2, 6	26, 30, 31, 36	
4	46		coil-loop: lc1'	0.6			1				
5	53	SER	coil-loop: lc2	0.6		1	3		2	36	
6	54	SER	coil-loop: lc2	1.5		1			2		
7	55	GLN	α LNop: lc2	2.7		1			2		
8	62	CYS	coil-loop: lc5	6.4		1			6	19	ALA[3] SER[4]
9	63*	ASP	coil-loop: lc5	10.8						19	
10	71*	LEU	coil-loop: lc6	406.1						10	
11	76*	LYS	α YS.1: lcB'	971.8						10	SER[5-6]
12	80*	ASP	α SPDIN EN.C	1146.3						10	PRO[5-6]
13	84*	ASP	coil-loop:	1706.5					1	6	THR[5-6]

			lc7									
14	95*	ASN	α SNDIN E C	3027.6					1			
15	96*	TRP	α RP7.6 E C	398.3							5	ALA/ PHE/ TYR[4, 7-8]
16	100*	HIS	α IS*-8 EN.	34950.4	X						5	ARG[9-10]
17	105*	PRO	3_{10}-helix: a	470.2	X				5			
18	106*	SER	3_{10}-helix: a	46.9					5		12	ARG[10]
19	109	GLN	coil-loop: lc8	4.0	X				5		37	LEU[9]
20	110	GLN	coil-loop: lc8	2.1	X						12	HIS[9]
21	143	GLU	α LUDIN E E	0.1		4			4, 10		3, 9, 16, 25, 37	GLY[9]
22	147	ARG	α RGDIN E E	0.1					4		7	
23	159	ASN	coil-loop: lc10	5.0			4					ASP[7]
24	182	ASP	α -helix: F	0.2		3					27, 29	VAL[9]
25	208	ASP	α -helix: G	0.3				1				
26	217	ASP	α -helix: G	0.5				3				VAL[11]
27	231	ASP	coil-loop: lc12	0.8		3, 5	4		3, 7, 9		2, 11, 12, 13, 18, 21, 22, 27, 37, 39	GLY[9]
28	236	HIS	α -helix: H	0.8			4					ARG[11] GLN[12]
29	243	PRO	coil-loop: lc13	1.4	X						8, 12, 22	
30	244*	GLU	coil-loop: lc13	297.3	X						5, 8	
31	247	GLU	coil-loop: lc13	0.1							8	
32	251	ASP	α SPop: 1 I	1.1				3			40	GLY[13]
33	253*	ASN	α SN*IN E I	259.6					1		6	
34	267	GLU	α LU.6N E I	0.2							29	GLN[14]

35	319	ASN	α SNDIN E K	0.7	X					4, 17, 20, 23, 32	SER[13]
36	337	GLU	coil-loop: lc18	0.4					8	17, 24, 31	
37	338	ASP	coil-loop: lc18	0.5			4				GLY[15]
38	348	GLU	coil-loop: lc20	1.4		1	4				
39	349	LYS	coil-loop: lc20	0.6		1					ASN[16]
40	351*	ASP	coil-loop: lc20	27.7		1			6	14, 35	
41	359*	GLN	α -helix: K'	156.3		3					
42	363	ASP	coil-loop: lc21	4.3		3			2	31, 33, 36	HIS[17]
43	372	GLU	coil-loop: lc22	0.3					8	17, 28, 33	CYS[18]
44	383	SER	3_{10}-helix: f	0.2						28	
45	386	PRO	coil-loop: lc22	0.1						28	SER[19]
46	388*	HIS	coil-loop: lc22	468.6	X					19	
47	397*	GLN	Cys-pocket: p1	1321.9	X					5	
48	407	LEU	α EU1.9t: L	0.5						32	
49	408	HIS	α IS1.9t: L	1.5						32	GLN[9]
50	436	THR	b-sheet: 4.1	0.3					8	4, 17, 29, 34	
51	440*	LYS	b-sheet: 4.2	31.3						29	ASN[20]

Table S6a. ET pathways with $k_{ET} > 10\ s^{-1}$ obtained from the 5CoS simulations

No. of ET Pathway	Co(II)Sep	Unique ET Pathways	Average k_{ET} (s^{-1})	Occurrence
1	1	D351→E352→L353→L333→S332→HEME	256.75	4
2		D351→A335→Y334→L333→S332→HEME	195.68	9
3	3	D363→L360→H361→I351→HEME	15.01	1
4		A34→E359→P358→I357→HEME	11.15	1
5		A34→A335→P358→I357→HEME	18.52	2
6	4	D231→S106→F107→HEME	10.13	1
7		D231→S106→F107→S108→ I401→C400→HEME	108.92	1
8		D159→L155→C156→T152→I153→HEME	11.34	1

Table S6b. ET pathways with $k_{ET} > 10\ s^{-1}$ obtained from the 10CoS simulation

No. of ET Pathway	Co(II)Sep	Unique ET Pathways	Average k_{ET} (s^{-1})	Occurrence
1	1	N253→N95→W96→HEME	70.19	1
2		N95→D84→G85→L86→HEME	32.85	1

3		N95→W96→HEME	4025.80	3
4		D84→N95→W96→HEME	2418.40	1
5		D84→G85→ L86→HEME	1595.48	17
6		D84→G85→ L86→F87→HEME	11.12	1
7	5	Q109→S108→F107→Q404→Q403 → G402→I401→C400→HEME	37.47	1
8		P105→L104→Q403→I401→C400→ HEME	470.23	3
9		S106→F107→I401→C400→HEME	70.76	15

Table S6c. ET pathways with $k_{ET} > 10\ s^{-1}$ obtained from the 40CoS simulation

No. of ET Pathway	Co(II)Sep	Unique ET Pathways	Average k_{ET} (s^{-1})	Occurrence
1	5	Q397→R398→A399→C400→HEME	1321.85	1
2		E244→N101→H100→HEME	564.53	4
3		H100→HEME	11135.08	11
4		H100→I401→C400→HEME	78611.77	6
5		W96→HEME	398.33	2
6	6	N253→N95→W96→HEME	188.94	2

7		N253→Q257→L86→HEME	342.20	4
8		D84→G85→L86→HEME	1852.15	18
9		D84→G85→T88→F87→R398→HEME	3658.27	1
10	10	D80→K76→S72→HEME	1146.29	2
11		L71→S72→HEME	406.14	5
12		K76→F77→Q73→S72→HEME	62.69	1
13		K76→S72→HEME	1025.27	17
14	14	D351→A335→Y334→L333→S332→S72→HEME	43.71	15
15	19	D63→S65→E64→Q397→R398→A399→C400→HEME	32.93	2
16		C62→G396→N395→G394→F393→C400→HEME	19.93	1
17		H388→N395→G394→F393→C400→HEME	733.73	7
18	38	D23→Q73→S72→HEME	141.22	18
19		D23→K24→D23→Q73→S72→HEME	497.18	4

Table S7a: Co(II)Sep unbound/bound interaction energies for 5CoS and 10CoS simulations. The values in bold highlight the Co(II)Sep molecules involved in the pathways reported in Table S5 and Figure S5. All energies are given in kJ/mol. The binding energy (DE) is defined as the difference between the average potential energy for the Co(II)Sep ion in the bound and unbound state.

	Simulations							
	5CoS I		*5CoS II*		*5CoS III*		*10CoS*	
	Unbound: -270±15		*Unbound:* -276±14		*Unbound:* -280±16		*Unbound:* -278±13	
CoSep	**Bound**	**DE**	**Bound**	**DE**	**Bound**	**DE**	**Bound**	**DE**
1	–349±19	-79±24	**–338±21**	**-68±25**	–360±17	-90±23	**–350±18**	**-80±22**
2	–335±20	-65±25	–367±19	-97±24	–343±17	-73±25	–380±16	-110±20
3	–366±16	-96±22	**–389±15**	**-119±20**	–371±15	-101±21	–348±19	-78±22
4	–330±17	-60±23	**–338±20**	**-68±25**	–366±15	-96±21	–402±19	-132±22
5	–370±17	-100±23	–355±28	-85±31	–414±16	-144±22	**–343±15**	**-73±20**
6							–346±17	-76±21
7							–328±17	-58±21
8							–367±17	-97±21
9							–342±17	-72±21
10							–353±18	-83±22

Table S7b: Co(II)Sep unbound/bound interaction energies for 40CoS simulation. The values in bold highlight the Co(II)Sep molecules involved in the pathways reported in Table S5 and Figure S5. The energies are given in kJ/mol. The binding energy (DE) is defined as the difference between the average potential energy for the Co(II)Sep ion in the bound and unbound state.

	CoSep molecule *Unbound state energy*: **-276±13**							
No.	1-10		11-20		21-30		31-40	
	Bound	**DE**	**Bound**	**DE**	**Bound**	**DE**	**Bound**	**DE**
1	–276±16	-6±20	–333±21	-63±25	–382±19	-112±22	–327±35	-57±37
2	–323±24	-53±27	–369±20	-99±24	–351±18	-81±22	–356±17	-86±21
3	–316±17	-46±21	–295±26	-25±29	–366±15	-96±20	–326±24	-56±27
4	–349±17	-79±21	**–347±16**	**-77±20**	–325±16	-55±20	–366±16	-96±20
5	**–344±18**	**-74±22**	–283±22	-13±26	–346±22	-76±26	–336±19	-66±22
6	**–349±18**	**-79±22**	–334±18	-64±22	–346±18	-76±22	–367±16	-97±20
7	–387±16	-117±20	–376±15	-106±20	–335±18	-65±22	–331±19	-61±22
8	–336±20	-66±24	–342±20	-72±24	–368±16	-98±20	**–351±17**	**-81±21**
9	–365±19	-95±22	**–357±18**	**-87±22**	–343±19	-73±22	–284±22	-14±26
10	**–344±16**	**-74±20**	–319±16	-49±20	–320±18	-50±22	–362±15	-92±20

FIGURES

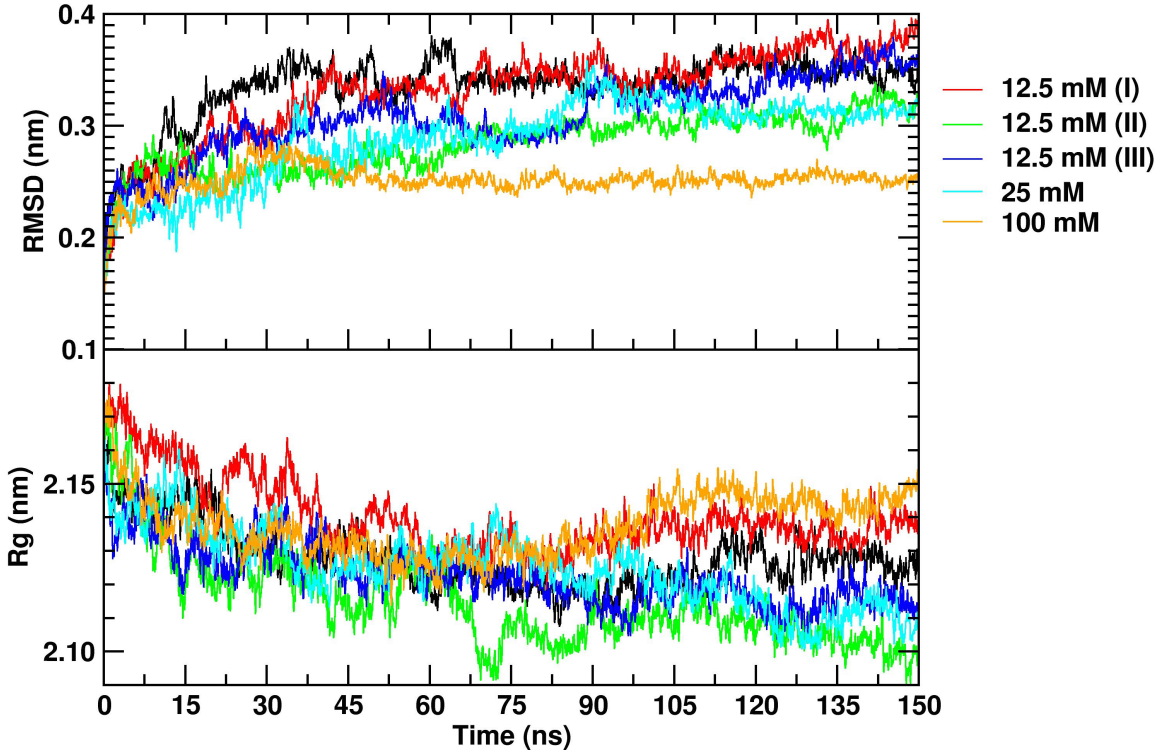

Figure S1: Radius of gyration and backbone root mean square deviation with respect to crystal structure as a function of time for HEME in water and at 12.5 mM (I-III), 25.0 mM and 100.0 mM Co(II)Sep concentrations in black, red, green, blue, cyan and orange color, respectively.

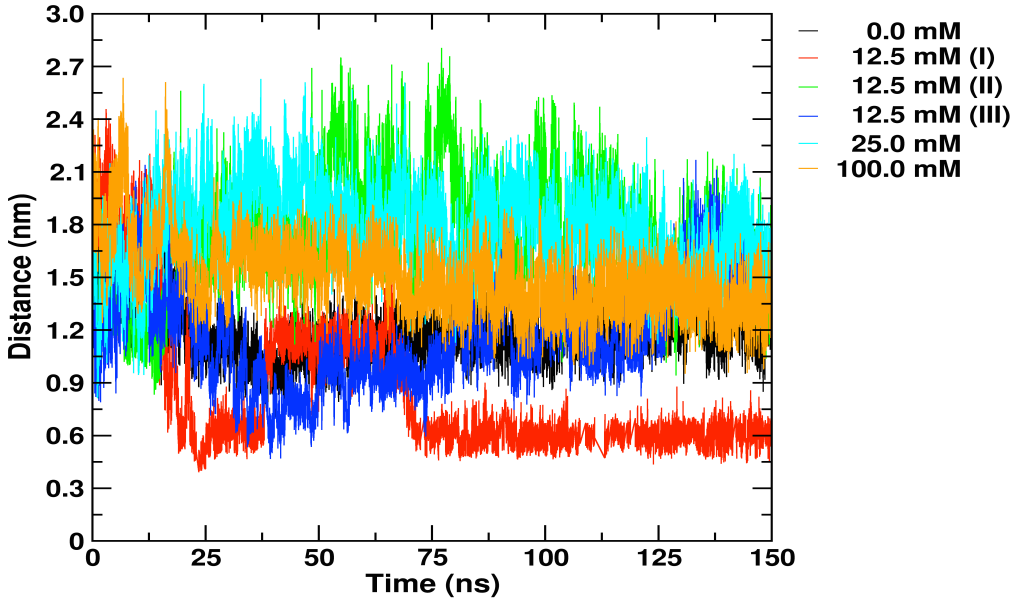

Figure S2: Minimum distance between P45C_α and A191C_α (1.61 nm in crystal structure) as a function of time for the simulations of HEME in the water (black color) and the water-Co(II)Sep solutions at 12.5 (I-III) mM, 25.0 mM and 100 mM concentrations in red, green, blue, cyan and orange color, respectively.

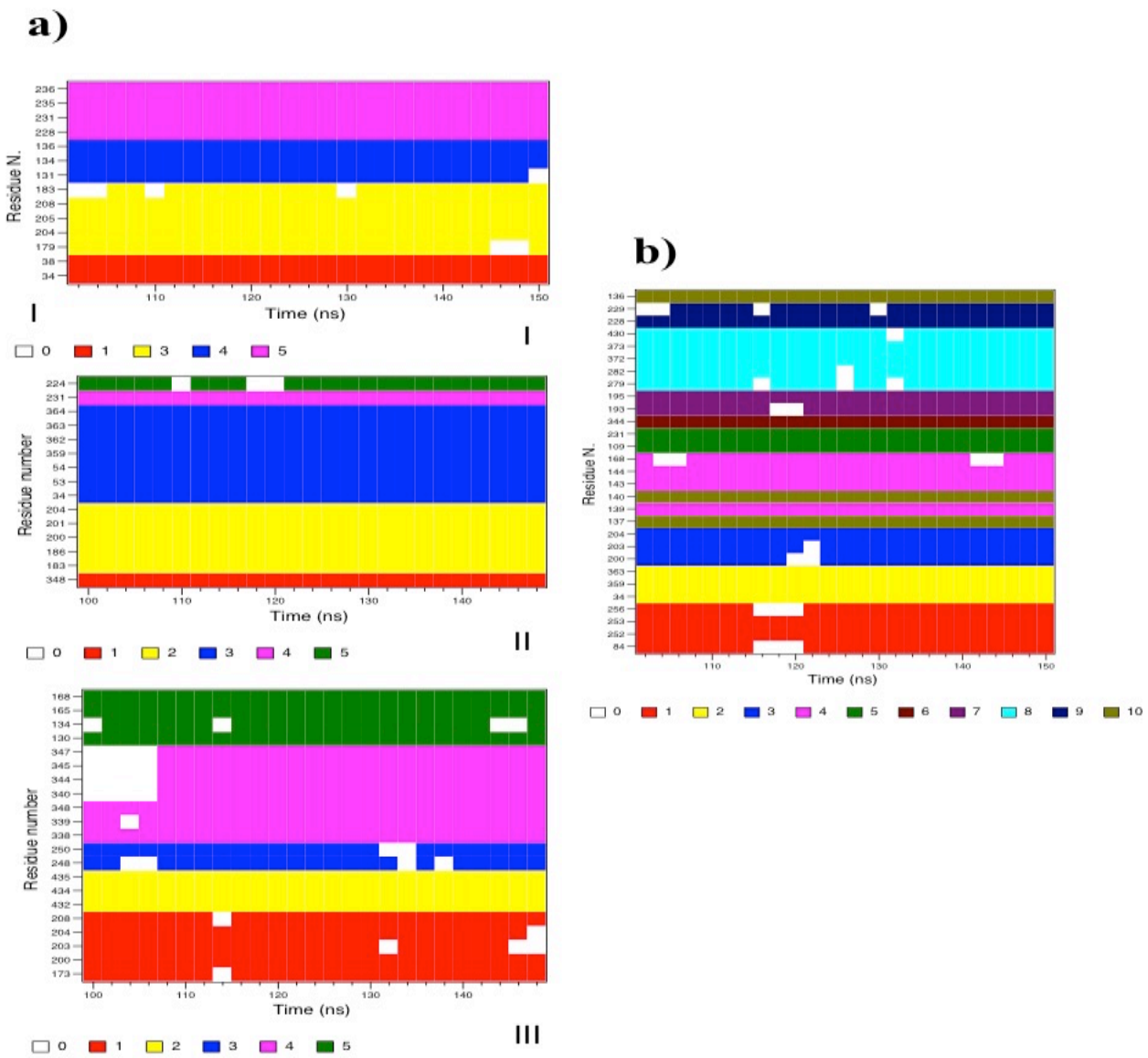

Figure S3a: Diagram of contact occurrences (number of contacts > 6) of the Co(II)Sep molecules (color coded) with the HEME residues in the last 50 ns simulation of **(a)** 5CoS (I-III) and **(b)** 10CoS. Only the residues with a percentage number of contact occurrence along the trajectory larger than 80% are reported.

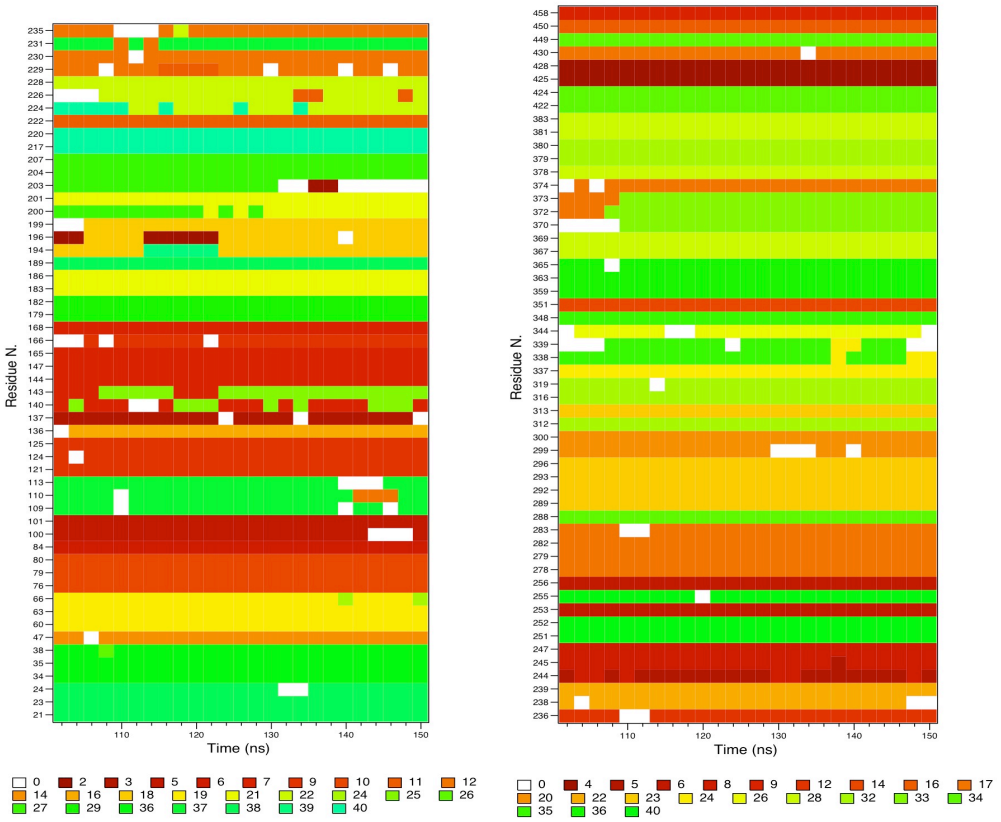

Figure S3b: Diagram of contact occurrences (number of contacts > 6) of the Co(II)Sep molecules (color coded) with the HEME residues in the last 50 ns simulation of 40CoS. Only the residues with a percentage number of contact occurrence along the trajectory larger than 80% are reported.

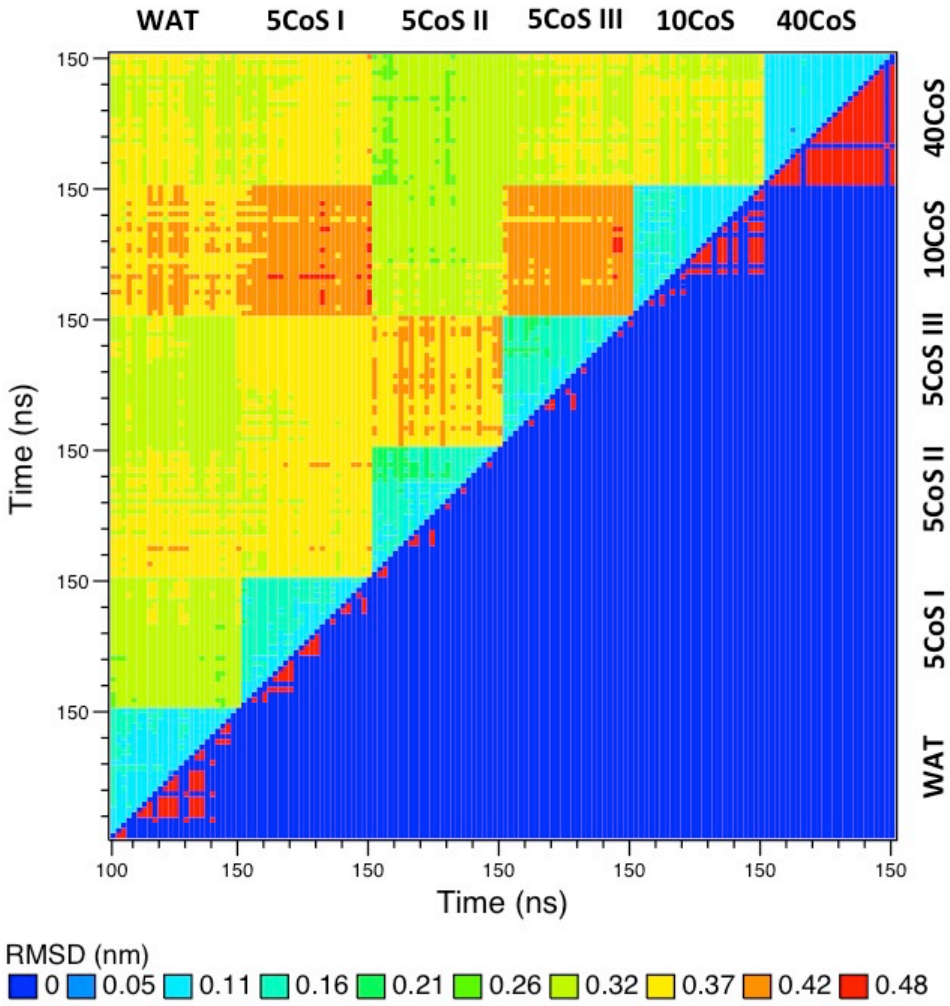

Figure S4: Upper triangular matrix shows the backbone RMSD matrix between the conformations in the combined trajectory formed by taking 25 conformations sampled every 2 ns frame from the last 50 ns of the four simulations. Lower triangular matrix has the clusters obtained from the cluster analysis of the conformations.

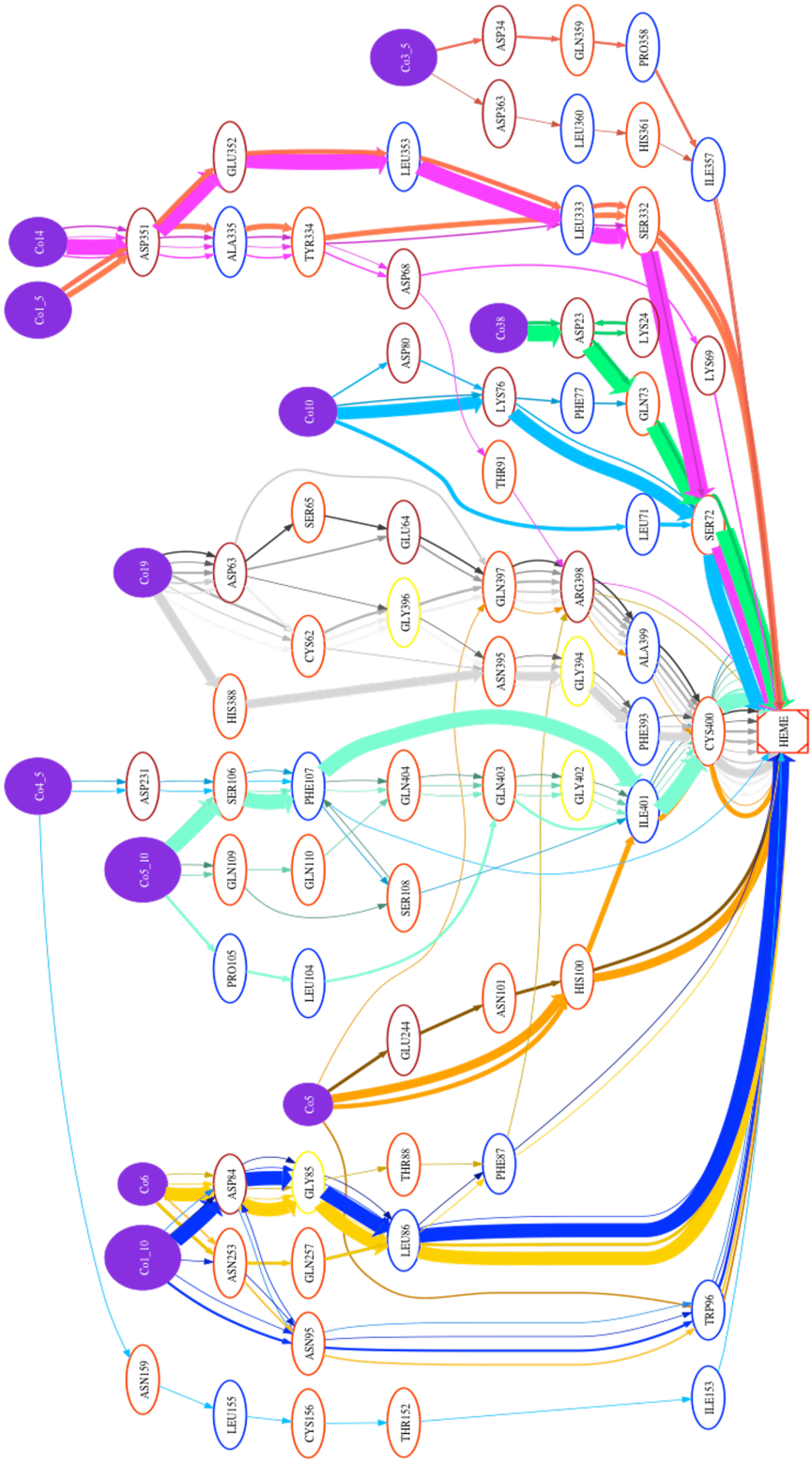

Figure S5: Combined representation of ET pathways with $k_{ET} \geq 10$ s^{-1} and occurring more than one time obtained from 5CoS, 10CoS and 40CoS simulation. The pathways are indicated using

different colors and line thickness that represents the number of conformations in which the pathway was observed. The color of ellipse around the amino acids names reflects the chemical nature of the amino acid (red: polar, brown: charged, blue: hydrophobic and aromatic; yellow: glycine).

REFERENCES

1. Dehayes, L. J.; Busch, D. H., Conformational Studies of Metal-Chelates .1. Intra-Ring Strain in 5-Membered and 6-Membered Chelate Rings. *Inorganic Chemistry* **1973,** *12*, 1505-1513.

2. van Gunsteren, W. F.; Billeter, S. R.; Eising, A. A.; Hunenberger, P. H.; Kruger, P.; Mark, A. E.; Scott, W. R. P.; Tironi, I. G., Biomolecular Simulation: The GROMOS96 Manual and User Guide. *VdF: Hochschulverlag AG an der ETH Zurich and BIOMOS b.v, Zurich, Groningen*. **1996**.

3. Ener, M. E.; Lee, Y. T.; Winkler, J. R.; Gray, H. B.; Cheruzel, L., Photooxidation of cytochrome P450-BM3. *Proc. Natl. Acad. Sci. U. S. A.* **2010,** *107*, 18783-18786.

4. Ferrero, V. E.; Andolfi, L.; Di Nardo, G.; Sadeghi, S. J.; Fantuzzi, A.; Cannistraro, S.; Gilardi, G., Protein and electrode engineering for the covalent immobilization of P450 BMP on gold. *Anal. Chem.* **2008,** *80*, 8438-8446.

5. Chen, C. K.; Shokhireva, T.; Berry, R. E.; Zhang, H.; Walker, F. A., The effect of mutation of F87 on the properties of CYP102A1-CYP4C7 chimeras: altered regiospecificity and substrate selectivity. *J. Biol. Inorg. Chem.* **2008,** *13*, 813-824.

6. Murataliev, M. B.; Trinh, L. N.; Moser, L. V.; Bates, R. B.; Feyereisen, R.; Walker, F. A., Chimeragenesis of the fatty acid binding site of cytochrome P450BM3. Replacement of residues 73-84 with the homologous residues from the insect cytochrome P450 CYP4C7. *Biochemistry* **2004,** *43*, 1771-1780.

7. Lewis, J. C.; Bastian, S.; Bennett, C. S.; Fu, Y.; Mitsuda, Y.; Chen, M. M.; Greenberg, W. A.; Wong, C. H.; Arnold, F. H., Chemoenzymatic elaboration of monosaccharides using engineered cytochrome P450BM3 demethylases. *Proc. Natl. Acad. Sci. U. S. A.* **2009,** *106*, 16550-16555.

8. Munro, A. W.; Malarkey, K.; McKnight, J.; Thomson, A. J.; Kelly, S. M.; Price, N. C.; Lindsay, J. G.; Coggins, J. R.; Miles, J. S., The role of tryptophan 97 of cytochrome P450 BM3 from Bacillus megaterium in catalytic function. Evidence against the 'covalent switching' hypothesis of P-450 electron transfer. *Biochem. J.* **1994,** *303 (Pt 2)*, 423-428.

9. Rentmeister, A.; Brown, T. R.; Snow, C. D.; Carbone, M. N.; Arnold, F. H., Engineered Bacterial Mimics of Human Drug Metabolizing Enzyme CYP2C9. *Chemcatchem* **2011,** *3*, 1065-1071.

10. Salazar, O.; Cirino, P. C.; Arnold, F. H., Thermostabilization of a cytochrome p450 peroxygenase. *Chembiochem* **2003,** *4*, 891-893.

11. Munzer, D. F.; Meinhold, P.; Peters, M. W.; Feichtenhofer, S.; Griengl, H.; Arnold, F. H.; Glieder, A.; de Raadt, A., Stereoselective hydroxylation of an achiral cyclopentanecarboxylic acid derivative using engineered P450s BM-3. *Chem. Commun.* **2005**, 2597-2599.

12. Farinas, Edgardo T.; Schwaneberg, U.; Glieder, A.; Arnold, Frances H., Directed Evolution of a Cytochrome P450 Monooxygenase for Alkane Oxidation. *Adv. Synth. Catal.* **2001,** *343*, 601-606.

13. Gilardi, G.; Meharenna, Y. T.; Tsotsou, G. E.; Sadeghi, S. J.; Fairhead, M.; Giannini, S., Molecular Lego: design of molecular assemblies of P450 enzymes for nanobiotechnology. *Biosens. Bioelectron.* **2002,** *17*, 133-145.

14. Yeom, H.; Sligar, S. G., Oxygen activation by cytochrome P450BM-3: effects of mutating an active site acidic residue. *Arch. Biochem. Biophys.* **1997,** *337*, 209-216.

15. Sawayama, A. M.; Chen, M. M.; Kulanthaivel, P.; Kuo, M. S.; Hemmerle, H.; Arnold, F. H., A panel of cytochrome P450 BM3 variants to produce drug metabolites and diversify lead compounds. *Chem.-Eur. J.* **2009,** *15*, 11723-11729.

16. Rentmeister, A.; Arnold, F. H.; Fasan, R., Chemo-enzymatic fluorination of unactivated organic compounds. *Nat. Chem. Biol.* **2009,** *5*, 26-28.

17. Nazor, J.; Dannenmann, S.; Adjei, R. O.; Fordjour, Y. B.; Ghampson, I. T.; Blanusa, M.; Roccatano, D.; Schwaneberg, U., Laboratory evolution of P450 BM3 for mediated electron transfer yielding an activity-improved and reductase-independent variant. *Protein Eng. Des. Sel.* **2008,** *21*, 29-35.

18. Sevrioukova, I. F.; Hazzard, J. T.; Tollin, G.; Poulos, T. L., The FMN to heme electron transfer in cytochrome P450BM-3. Effect of chemical modification of cysteines engineered at the FMN-heme domain interaction site. *J. Biol. Chem.* **1999,** *274*, 36097-36106.

19. Eiben, S.; Kaysser, L.; Maurer, S.; Kuhnel, K.; Urlacher, V. B.; Schmid, R. D., Preparative use of isolated CYP102 monooxygenases -- a critical appraisal. *J. Biotechnol.* **2006,** *124*, 662-669.

20. Li, H. M.; Mei, L. H.; Urlacher, V. B.; Schmid, R. D., Cytochrome P450 BM-3 evolved by random and saturation mutagenesis as an effective indole-hydroxylating catalyst. *Appl. Biochem. Biotechnol.* **2008,** *144*, 27-36.